1

Introduction

For more than a century, scientists and engineers have used the interference of light waves to assess the optical properties of an object (Lauterborn *et al.*, 1993; Monnier, 2003; Saha, 2002). A well-known example of an optical interference pattern is Newton's rings, where light waves reflecting from two closely spaced surfaces interfere to form a ring pattern as shown in Figure 1.1.

The intensity pattern $|D(\mathbf{A})|^2$ is known as an interferogram, where $D(\mathbf{A})$ describes the brightness field at a location $\mathbf{A}$ on the top of the lens surface. The interferogram characterizes the interference between the upgoing reflections from the bottom of the lens at $\mathbf{B}$ and from the glass pane at $\mathbf{C}$. Dark rings correspond to zones where the reflections with raypaths ABA and ACA are out of phase resulting in destructive interference, while the bright rings correspond to the in-phase reflections that give rise to constructive interference. The phase is controlled by the lens thickness, which thickens toward the center, so that any departures from perfect circular rings indicate subtle variations from an ideal lens geometry. As an example, Figure 1.2 shows an interferogram that reveals micron-sized imperfections in a cut diamond, where micron-deep pits show up as triangular interference patterns.

1.1 Seismic interferometry

Analogous to optical interferometry, seismic interferometry estimates the detailed properties of the Earth by analyzing the interference patterns of seismic waves. These patterns are constructed by correlating and summing pairs of seismic traces with one another to robustly image the Earth's elastic properties. As an example, consider the Figure 1.3a Earth model where single-channel seismic traces are recorded over a sand lens underlying a complex overburden. There are two events in each seismogram, the early one is the upgoing reflection from the top of the sand lens and the later one is the reflection from the bottom of the sand lens. The

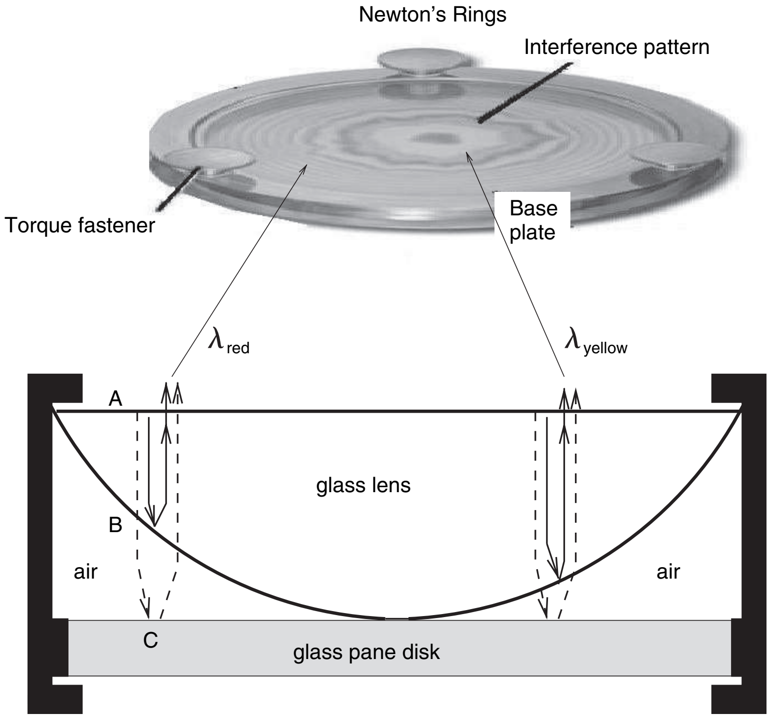

Fig. 1.1 Newton's rings are formed by optical interference of reflections from the lens-air and air-pane interfaces. Constructive interference results for a certain color if the phase difference between the reflections with paths ABA and ACA is an integer multiple of a wavelength for that color.

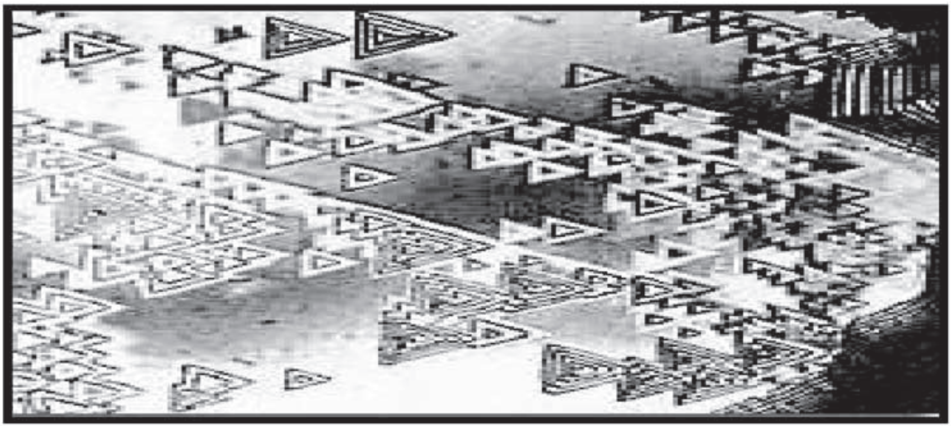

Fig. 1.2 Interferogram obtained by shining 0.5 micrometer wavelength light on a diamond overlying a glass pane. The small triangular interference patterns are associated with 0.12 micrometer deep pits on the diamond's surface. (Image obtained from the Nikon microscope website www.microscopyu.com/articles/interferometry/twobeam.html.)

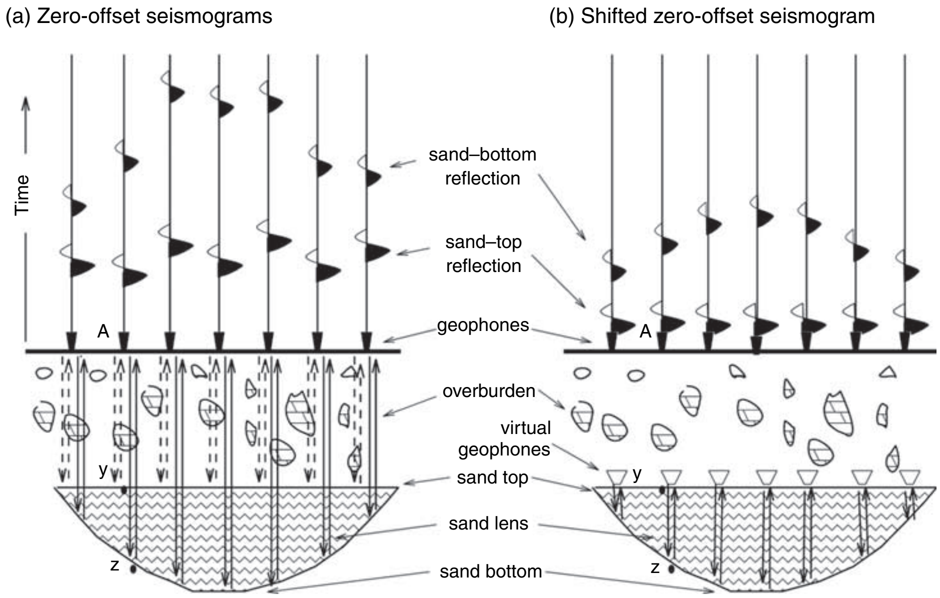

Fig. 1.3 (a) Zero-offset reflection seismograms are shown above a sand lens with an irregular overburden. Each trace is recorded with both the source and geophone at the same location on the surface of the Earth; and a 1D wave propagation model is assumed with only vertically traveling waves. The reflections from the top and bottom of the sand lens vary in time as a function of trace location on the surface; and the temporal variations are due to the irregular transit times through the inhomogeneous overburden (characterized by the irregular shapes in the overburden). (b) Reflection seismograms shifted by the traveltimes of the sand-top reflections remove the timing irregularities. See Appendix 1 for further details of a seismic experiment.

goal here is to determine the geometry of the sand lens, which is similar to that of an explorationist who is hunting for oil-sopped sand bodies (see Appendix 1 for a basic background on seismic experiments).

Unfortunately, the shape of the sand lens suggested by the seismograms is distorted because of the lateral velocity variations in the overburden. Such distortions are sometimes referred to as statics, not unlike the distorted image of a fish seen from above a choppy lake surface. To remove these static distortions, notice that the vertical transit time through the overburden is equal to the traveltime τ_{AyA} of the reflection from the top of the sand lens. Here, τ_{AyA} denotes the traveltime of a reflection wave propagating from A on the surface to y at the top of the lens and back to A; and the raypath of this reflection is denoted by the dashed arrows. Notice that τ_{AyA} varies from trace to trace and defines the overburden statics. *Shifting each trace by* τ_{AyA} *removes the overburden's statics to give the undistorted seismograms in Figure 1.3b, which are kinematically* *similar to traces obtained from virtual sources and receivers shifted to the top of the lens.* It is equivalent to applying statics corrections to land data (Yilmaz, 2001). Similar to the optical interferometry example, the time-differenced seismograms in Figure 1.3b reveal the lens geometry free of the distorting effects of the overburden.

Mathematical description For purposes of illustration, one of the traces in Figure 1.3a is extracted and shown on the left-hand side of Figure 1.4. The middle panel only contains the reflection from the top of the lens; and its reflection arrival time τ_{AyA} is used to time shift the leftmost seismogram to give the one on the far right. As will now be shown using a Dirac delta function, time shifting is roughly equivalent to correlating a pair of traces with one another.

Dirac delta function

The Dirac delta function is defined by taking the limit of a sequence of strongly peaked functions $\phi_n(t)$ (for $n = 1, 2, 3, \ldots$) that peak at the argument $t = 0$ (Butkov, 1972). This gives a function that is effectively zero everywhere except when the argument is zero and so enjoys the sifting property. For example, the unit-advance operator $\delta(t+1)$ (which peaks at $t = -1$) has the property of advancing the input time signal $f(t)$ by one time unit to an earlier time, i.e.,

$$f(t+1) = f(t) \star \delta(t+1) = \int_{-\infty}^{\infty} f(t-\tau)\delta(\tau+1)d\tau, \tag{1.1}$$

where $\star$ denotes convolution. Similarly, the unit delay operator $\delta(t-1)$ delays the input signal by one time unit:

$$f(t-1) = f(t) \star \delta(t-1) = \int_{-\infty}^{\infty} f(t-\tau)\delta(\tau-1)d\tau. \tag{1.2}$$

More generally, $\delta(t+|\tau|)$ can be thought of as an acausal function because it advances the input signal by convolution to an earlier time, while $\delta(t-|\tau|)$ delays the input signal by $|\tau|$ to a later time. In the real-time world, the Earth is a causal system because it always delays the input signal (such as an earthquake propagating to a distant receiver) and never advances it in time. That is, we never feel the earthquake prior to its rupture time.

Assume an impulsive source described by the Dirac delta function $\delta(t)$ (Butkov, 1972), so that the leftmost reflection trace in Figure 1.4 is represented by the zero-offset data $d(\mathbf{A}, t|\mathbf{A}, 0)$:

$$d(\mathbf{A}, t|\mathbf{A}, 0) = \overbrace{\delta(t-\tau_{AyA})}^{\textit{top-of-sand refl.}} + \overbrace{\delta(t-\tau_{AzA})}^{\textit{bottom-of-sand refl.}}, \tag{1.3}$$

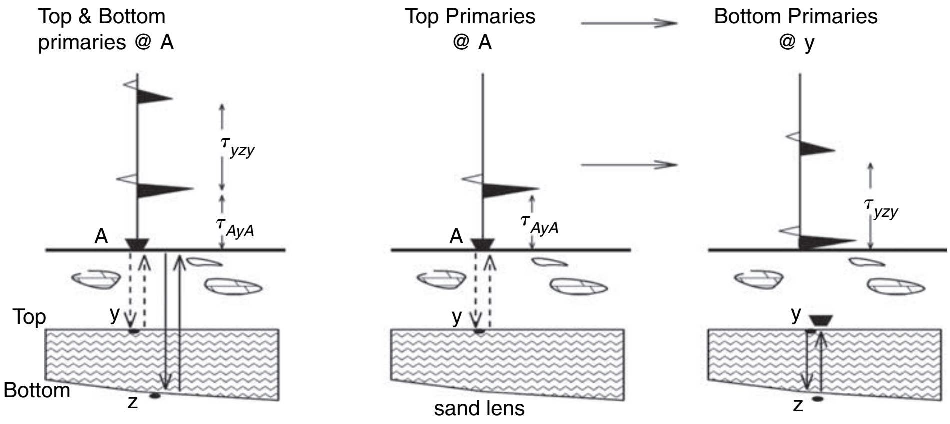

Fig. 1.4 Time shifting the leftmost reflection trace by τ_{AyA} yields the trace on the far right. This time-shifted trace is kinematically equivalent to the one recorded by a receiver (and a source) buried at depth **y**. The time shifting operation is roughly the same as a correlation of the far left and middle traces (Appendix 2).

where the reflection coefficients are assumed to be unity and the direct wave is muted. The notation for $d(\mathbf{A}, t|\mathbf{A}, 0)$ says that the coordinate vector **A** to the right of the vertical bar represents the source location while the vector to the left is the receiver location. Unless noted otherwise, the source initiation time is always assumed to be at time zero, the observation time is denoted by t, and vectors will be denoted by boldface letters. For notational simplicity, geometrical spreading and reflection coefficient effects are suppressed by assuming a trace normalization procedure (Yilmaz, 2001) such as an AGC (automatic gain control). More generally, the exact wavefield excited by an impulsive point source (which is a line source in 2D) at **B** with initiation time t_s and an observer at **A** is described by the Green's function $g(\mathbf{A}, t|\mathbf{B}, t_s)$ (Morse and Feshback, 1953).

The Fourier transform[1] of $d(\mathbf{A}, t|\mathbf{A}, 0)$ is equal to

$$D(\mathbf{A}|\mathbf{A}) = \frac{1}{2\pi}[e^{i\omega\tau_{AyA}} + e^{i\omega\tau_{AzA}}], \qquad (1.4)$$

where $D(\mathbf{A}|\mathbf{A})$ is the Fourier spectrum of the seismogram $d(\mathbf{A}, t|\mathbf{A}, 0)$ with the angular frequency variable suppressed. Shifting the seismograms by τ_{AyA} is equivalent to multiplying the spectrum $D(\mathbf{A}|\mathbf{A})$ by $e^{-i\omega\tau_{AyA}}$ to give the shifted spectrum $D(\mathbf{A}|\mathbf{A})' = D(\mathbf{A}|\mathbf{A})e^{-i\omega\tau_{AyA}} = [1 + e^{i\omega(\tau_{AzA}-\tau_{AyA})}]/(2\pi)$. To form an interferogram similar to the optical lens example, calculate the weighted intensity (or squared

[1] See Appendix 2 for the definition of the Fourier transform and some useful identities.

magnitude spectrum) of $D(\mathbf{A}|\mathbf{A})'$ as

$$\begin{aligned} 4\pi^2|D(\mathbf{A}|\mathbf{A})'|^2 = 4\pi^2 D(\mathbf{A}|\mathbf{A})' D(\mathbf{A}|\mathbf{A})'^* &= |1+e^{i\omega(\tau_{AzA}-\tau_{AyA})}|^2 \\ &= 2+2\cos(\omega(\tau_{AyA}-\tau_{AzA})) \\ &= 2+2\cos(\omega\tau_{yzy}), \end{aligned} \tag{1.5}$$

where $\tau_{yzy} = 2|z-y|/v$ is the two-way vertical traveltime in the sand lens, v represents the P-wave velocity in the sand, $*$ indicates complex conjugation, and $|z-y|$ is the lens thickness.

Similar to the relationship between the optical interferogram[2] and optical lens thickness, the spectral interferogram $|D(\mathbf{A}|\mathbf{A})'|^2$ in Equation (1.5) only depends on the transit time through the sand lens. *This means that $|D(\mathbf{A}|\mathbf{A})'|^2$ will be sensitive to any irregularities in the shape of the sand lens. Moreover, this spectral interferogram is kinematically equivalent to one recorded with source and receivers redatumed[3] to the top of the sand lens.* The next section shows this transformation to be equivalent to correlation in the time domain.

Convolution, cross-correlation, and autocorrelation

Convolution between two real functions $f(t)$ and $g(t)$ is defined in the time domain as

$$h(t) = f(t) \star g(t) = \int_{-\infty}^{\infty} f(\tau)g(t-\tau)d\tau, \tag{1.6}$$

where the symbol $\star$ denotes convolution. As shown in Appendix 2, the Fourier transform of $h(t)$ is given by the spectrum $H(\omega)$ at angular frequency ω:

$$H(\omega) = 2\pi F(\omega)G(\omega), \tag{1.7}$$

where the spectrums of $f(t)$ and $g(t)$ are denoted by $F(\omega)$ and $G(\omega)$, respectively. The correlation of two functions is defined as

$$h(t) = f(t) \otimes g(t) = f(-t) \star g(t) = \int_{-\infty}^{\infty} f(\tau)g(t+\tau)d\tau, \tag{1.8}$$

[2] The intensity of the upgoing harmonic lightwaves along the top of the optical lens in Figure 1.1 is similar in mathematical form to Equation (1.5) except $D(\mathbf{A}|\mathbf{A}) \approx e^{i\omega\tau_{AyA}} - e^{i\omega\tau_{AzA}}$; here, $AyA/2$ is the thickness of the lens below $\mathbf{A}$ and $AzA/2$ is the vertical distance between the glass pane and the point $\mathbf{A}$ on the lens surface. Therefore, τ_{AyA} and τ_{AzA} are, respectively, the two-way transit times through the lens and from the lens surface to the glass pane.

[3] The acquisition surface where sources and receivers are located is known as a datum. Transforming the traces such that they appear to have been recorded on a different acquisition surface is known as redatuming the traces. Transforming traces to a deeper datum can rectify imaging problems associated with near-surface velocity variations.

where the symbol $\otimes$ denotes correlation. For discretely sampled signals $f(t) \rightarrow [f(0)\, f(\Delta t)\, f(2\Delta t) \ldots f((N-1)\Delta t)] = \mathbf{f}$ and $g(t) \rightarrow \mathbf{g}$ with N time samples, $f(t) \otimes g(t)$ can be interpreted as the dot product of the $Nx1$ vector $\mathbf{f}$ with a time-shifted copy of the $Nx1$ vector $\mathbf{g}$. The time shift that leads to a large correlation value says that $\mathbf{f}$ and the time-shifted copy of $\mathbf{g}$ have a strong resemblance to each other. If $f(t) = g(t)$ then Equation (1.8) is known as autocorrelation, otherwise it is denoted as cross-correlation. As shown in Appendix 2, the Fourier transform of $f(t) \otimes g(t)$ is given by

$$H(\omega) = 2\pi F(\omega)^* G(\omega). \tag{1.9}$$

If $F(\omega) = G(\omega)$, then $H(\omega) = 2\pi |F(\omega)|^2$ is the squared magnitude spectrum of the autocorrelation function $f(t) \otimes f(t)$.

An important property of correlation is that the phases in the spectral product $2\pi F(\omega)^* G(\omega) = 2\pi |F(\omega)^*||G(\omega)| e^{i\omega(\tau_G - \tau_F)}$ are subtractive. Subtracting the traveltime τ_F from τ_G leads to smaller traveltimes and events with shorter raypaths. This is illustrated by shifting the traces in Figure 1.3a where the traveltime associated with the common raypath AyA is contracted to give shorter duration traces in Figure 1.3b. These shorter duration records are equivalent to ones obtained by redatuming the source and receiver to be closer to the sand lens.

Similarly, temporal convolution of $f(t)$ and $g(t)$ leads to the spectral product $2\pi F(\omega) G(\omega) = 2\pi |F(\omega)||G(\omega)| e^{i\omega(\tau_G + \tau_F)}$ with additive phases. This means that the resulting event has a longer traveltime than the events in $f(t)$ and $g(t)$, and this new event has a longer raypath. Figure 1.5 illustrates this concept for both convolution and correlation.

Traveltime shift $\leftrightarrow$ trace correlation Rather than manually shifting each trace by τ_{AyA} to remove the overburden statics, one can autocorrelate the traces. From Equation (1.9), the weighted Fourier transform $\mathcal{F}(\,)$ of the temporal autocorrelation function $d(\mathbf{A}, t|\mathbf{A}, 0) \bigotimes d(\mathbf{A}, t|\mathbf{A}, 0)$ is the squared magnitude spectrum:

$$\begin{aligned} \frac{1}{2\pi} \mathcal{F}(d(\mathbf{A}, t|\mathbf{A}, 0) \bigotimes d(\mathbf{A}, t|\mathbf{A}, 0)) &= D(\mathbf{A}|\mathbf{A}) D(\mathbf{A}|\mathbf{A})^* \\ &= |e^{i\omega\tau_{AyA}} + e^{i\omega\tau_{AzA}}|^2 \\ &= 2 + 2\cos(\omega\tau_{yzy}), \end{aligned} \tag{1.10}$$

which is equal to Equation (1.5) for the squared spectrum of the shifted traces. In this example autocorrelation of the traces is equivalent to removing the distorting effects of the overburden and redatuming the source and receivers to be just above the target body.

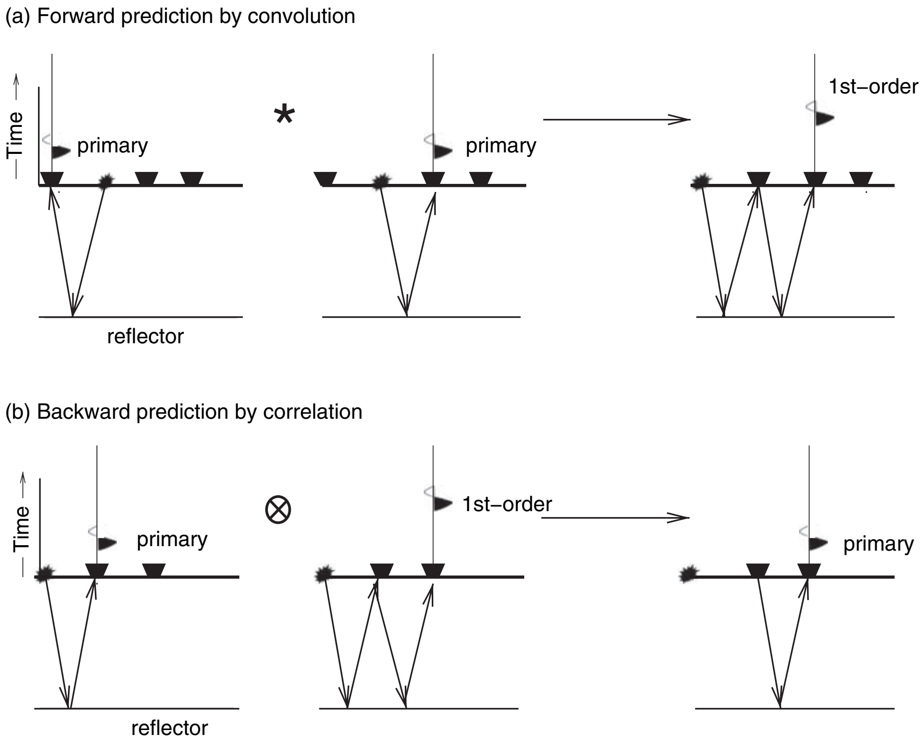

Fig. 1.5 (a) Convolution of traces creates events with longer traveltimes and raypaths and (b) correlation of traces creates events with shorter raypaths and traveltimes. For the correlation example, the source location at the left is redatumed to be at a geophone location on the right. The distortions of the wavelet due to geometric spreading, convolution, or correlation are conveniently ignored here and in subsequent chapters.

Often an explosive source is buried at a depth z_A to maximize the coupling between the explosion and the Earth. In this case the events in the Figure 1.3a seismograms will arrive earlier, but there will be no change in the shifted seismograms in Figure 1.3b. This is because the 2-way transit time in the overburden is removed by correlation as long as the source is buried no deeper than the lens. Therefore, the redatumed data can be summed[4] over N buried sources with depths denoted by z_A and still give a similar result:

$$\Phi(\mathbf{B}|\mathbf{A}) = \sum_{z_A} D(\mathbf{B}|\mathbf{A})D(\mathbf{B}|\mathbf{A})^*, \tag{1.11}$$

[4] Summation of in-phase signals increases the signal/noise ratio of noisy traces. Summation is also a necessary step for redatuming of non-zero offset traces as will be shown in the next section.

where $\mathbf{A} = (x_A, y_A, z_A)$ represents the source position and the receiver position at $\mathbf{B} = (x_A, y_A, 0)$ is just above the buried source position. The correlation function $\Phi(\mathbf{B}|\mathbf{A})$ is interpreted as redatumed data because its inverse Fourier transform $\mathcal{F}^{-1}(\,)$ is

$$\phi(\mathbf{B}, t|\mathbf{A}) = N[2\pi \overbrace{\delta(t + \tau_{yzy})}^{acausal} + \overbrace{4\pi\delta(t) + 2\pi\delta(t - \tau_{yzy})}^{causal}], \qquad (1.12)$$

where the causal part of this expression $4\pi\delta(t) + 2\pi\delta(t - \tau_{yzy})$ represents the data recorded by a source and receiver just above the sand lens. These data can then be used to image the reflectivity distribution by a process known as seismic migration.

1.1.1 Multidimensional seismic interferometry

The concept of redatuming by correlation is also valid for non-zero offset data as shown in Figure 1.6, except cross-correlated VSP traces rather than autocorrelated traces are used.[5] Here, correlation of the direct arrival $d(\mathbf{A}, t|\mathbf{x}, 0)$ at $\mathbf{A}$ with the ghost reflection[6] $d(\mathbf{B}, t|\mathbf{x}, 0)^{ghost}$ recorded at $\mathbf{B}$ exactly cancels the traveltime of the ghost

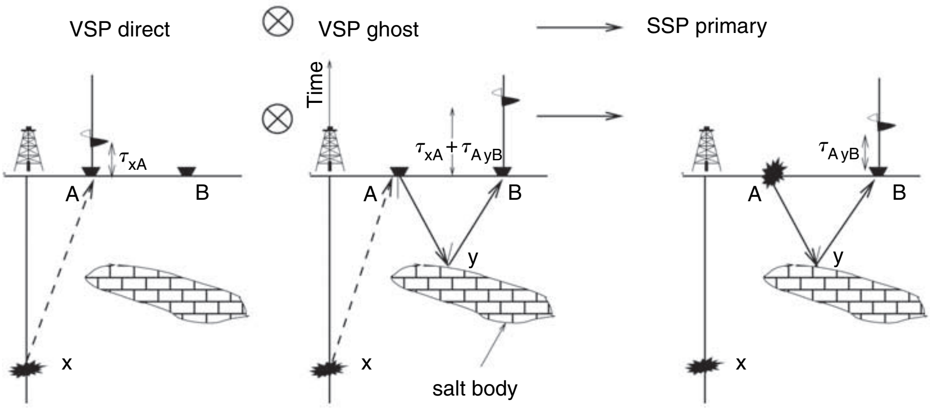

Fig. 1.6 Correlation of a ghost arrival at **B** with a direct arrival at **A** followed by summation over source locations at **x** yields the redatumed surface seismic profile (SSP) trace on the right $d(\mathbf{B}, t|\mathbf{A}, 0)$. In this case, the ghost has been converted to a primary, or more generally, vertical seismic profile (VSP) data have been converted to SSP data. Short bars indicate that Snell's law is honored at the reflection point; and the drilling well is indicated by the platform attached to the thick vertical line.

[5] To broaden our discussion we switch from the SSP geometry to the inverse VSP experiment without losing applicability to the SSP example. The inverse and standard VSP experiments will often be referred to as VSP experiments.

[6] A ghost reflection is an arrival from the subsurface that also reflected off the Earth's free surface; a primary reflection is one where a wave travels down to the reflector and back up to the receiver just once.

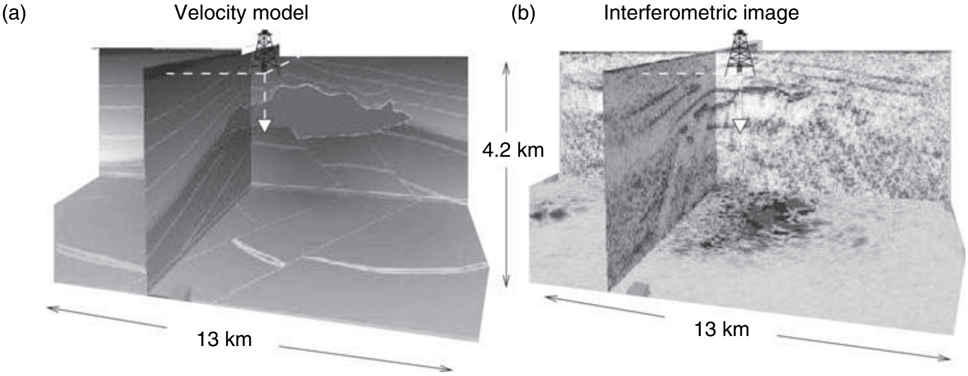

Fig. 1.7 Pictures of (a) a 3D salt velocity model and (b) the associated interferometric migration image obtained by migrating correlated traces from 6 receiver gathers; the receivers were spaced at 20 m along the well. Solid triangle denotes the approximate location of the 6 receivers and there is a 448 × 448 array of sources on the surface with a 30 m source spacing (adapted from He *et al.*, 2007).

along the common raypath xA. This results in the virtual surface seismic primary reflection, whose raypath is seen on the far-right ray diagram. In this case both sources and receivers are virtually located on the surface and can super-illuminate a much wider portion of the Earth compared to standard VSP imaging where the sources or receivers are confined to the well.

A dramatic example of super-illumination is the 3D interferometric migration image shown in Figure 1.7. Here, the reflectivity model is estimated by correlating, summing, and migrating just six receiver gathers of synthetic VSP traces. The sources were located just below the free surface and the shallowest VSP receiver was approximately positioned deeper than 1 km in the well. The coverage of the VSP interferometric image is comparable to a surface seismic survey around the well. In comparison, a standard VSP image only covers a small cone-shaped volume beneath the shallowest receiver.

The source position at **x** in Figure 1.6 is fortuitously placed so that the direct ray xA coincides with the first leg of the specular[7] ghost ray. This special source location **x** is called a stationary source position. To insure that a stationary source position is always found, the correlated records are summed (similar to Equation (1.11)) over different source positions in the well:

$$d(\mathbf{B}, t|\mathbf{A}, 0) \approx \sum_{\mathbf{x}\epsilon S_{well}} d(\mathbf{A}, t|\mathbf{x}, 0) \otimes d(\mathbf{B}, t|\mathbf{x}, 0)^{ghost}, \tag{1.13}$$

[7] Short bars indicate that Snell's law is honored, which means that portion of the ray is specular.